

# PRESTO, the on-line photon energy spectrometer at FERMI: design, features and commissioning results

Cristian Svetina,<sup>a,b,\*</sup> Daniele Cocco,<sup>c</sup> Nicola Mahne,<sup>a</sup> Lorenzo Raimondi,<sup>a</sup> Eugenio Ferrari<sup>a,d</sup> and Marco Zangrando<sup>a,e</sup>

<sup>a</sup>Elettra-Sincrotrone Trieste SCpA, SS 14 km, 163.5 in Area Science Park, Basovizza 34149, Italy, <sup>b</sup>Graduate School of Nanotechnology, University of Trieste, Piazzale Europa 1, Trieste 34127, Italy, <sup>c</sup>SLAC National Accelerator Laboratory, 2575 Sand Hill Road, Menlo Park, CA 94025, USA, <sup>d</sup>Department of Physics, University of Trieste, Via A. Valerio 2, Trieste 34127, Italy, and <sup>e</sup>IOM-CNR, Laboratorio TASC, SS 14 km 163.5 in Area Science Park, Trieste 34149, Italy.

\*Correspondence e-mail: cristian.svetina@elettra.eu

Measurement of the emission wavelength and the spectral content of the photon radiation is essential information for both machine and experimental physicists at a free-electron laser (FEL) user facility. Knowledge of the photon beam spectral properties is needed during the machine optimization and for performing machine studies (*i.e.* monitoring the change of the FEL output as a function of the machine parameters). The experimentalists, on the other hand, need to know the photon beam spectral distribution of the source, shot to shot, to discriminate the acquired data. Consequently, the main requirement for the instrument, supposed to obtain this information, is the capability of working on-line and shot-to-shot, with minimal perturbation of the beam delivered to the experimental stations. Starting from the grating fundamental equations, the conceptual design of the FERMI Pulse-Resolved Energy Spectrometer: Transparent and On-line (PRESTO) is presented, explaining the optical design in detail. The performance of PRESTO, in terms of resolving power, efficiency and spectral response, is also discussed. Finally, some useful features beyond the usual measurement of the energy spectrum are reported, as they have been routinely used by both machine and experimental physicists.

## 1. FERMI

FERMI is the first single-pass seeded free-electron laser (FEL) user facility in the VUV/soft X-ray range. It makes use of a high-gain harmonic generation (HG) (Allaria *et al.*, 2015) scheme and provides almost fully coherent and transform-limited photon pulses with 10 Hz repetition rate (to be increased to 50 Hz in the near future). It is composed of two separated undulator chains (FEL-1 and FEL-2), for covering a wide wavelength range: FEL-1 covers the low-energy range from 12 eV to 62 eV (20–100 nm) (Allaria *et al.*, 2010, 2012a) while FEL-2 is a double-stage cascade FEL covering the higher-energy range from 62 eV to 310 eV (4–20 nm) (Allaria *et al.*, 2013a). By using the FEL third harmonics the energy range covered by FERMI is extended to 930 eV (1.3 nm). The presence of variable-gap APPLEII undulators and the tunable seed laser allow the photon energy to be scanned continuously across the whole FERMI range. The polarization of the emitted FEL radiation can also be varied from linear (horizontal–vertical) to circular (left–right) as recently demonstrated by Allaria *et al.* (2014) and Finetti *et al.* (2014). The emitted radiation parameters are summarized in Table 1.

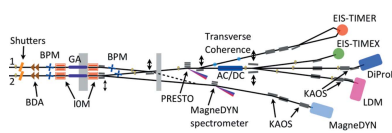


**Table 1**  
Main output parameters measured at FERMI during the commissioning of FEL-1 and FEL-2.

Parameter	FEL-1	FEL-2
Wavelength (nm)	100–20	20–4
Pulse length r.m.s. (fs)	30–100	<100
Spectral width $\Delta\lambda/\lambda$ FWHM	$10^{-3}$	$10^{-3}$
Central wavelength fluctuation	$<10^{-4}$	$<10^{-4}$
Energy per pulse ( $\mu\text{J}$ )	>100	20–100
Power fluctuation (%)	<25	<50
Polarization	Linear (H/V)– circular (L/R)	Linear (H/V)– circular (L/R)
Repetition rate (Hz)	10	10

**2. Photon analysis delivery and reduction system (PADReS)**

PADReS is the FERMI section devoted to the analysis of several parameters of the FEL output photon beam as well as to deliver the beam to the end-stations after proper manipulation. It is placed downstream of the two undulator chains and before the experimental end-stations. A schematic layout is shown in Fig. 1.

The system permits measurement, in a non-invasive way, of photon beam parameters like the beam position, the divergence, the angular jitter, the intensity and the photon energy spectrum. All of these are essential information provided during the users’ operations. The setups to measure the transverse coherence (double slits) and longitudinal coherence (AD/DC) are invasive as well as the screens for the transverse photon distribution characterization (mainly used for machine optimization and alignment purposes). There is also the possibility to reduce the overall FEL intensity or to transmit almost only the third harmonic by using the gas absorber (Rumiz *et al.*, 2011). The working principles of the various diagnostics as well as the commissioning results have already been explained in detail in previous papers (Zangrando *et al.*, 2009, 2014, 2015). The location of the diagnostics is shown in Fig. 1.

**3. Pulse-resolved energy spectrometer: transparent and on-line (PRESTO)**

The measurement of the FEL pulse-resolved spectral distribution, without perturbing the photon beam wavefront delivered to the end-stations, is not trivial and requires custom technical solutions. In order not to perturb the radiation delivered to the experiments, only a small fraction of the incoming radiation from the source is used. PRESTO has been designed in order to allow the accurate measurement of the photon energy spectral distribution over the whole FERMI energy range, including the third harmonic. The most important information directly obtained

by using this instrument is the energy distribution, in particular the central wavelength (peak position) and the bandwidth (FWHM) of the emitted radiation. Other useful information can also be obtained, and will be described in the following sections.

The instrument is similar to the FLASH spectrometer (Brenner *et al.*, 2011) but with three longer grazing-incidence flat variable-line-spacing (VLS) gratings that can be chosen according to the wavelength of the incoming radiation. With these three gratings PRESTO is able to cover the whole energy range of FERMI from 100 nm down to 1 nm. The reflected radiation (*e.g.* the zeroth-order of diffraction) is sent to the following beamlines, while the diffracted part of the radiation is focused to a triggered detector acquiring the single-shot images. While other methods could be used to characterize the spectral content (for instance a time-of-flight spectrometer), PRESTO has been considered the easiest option since the acquired data are immediately recorded and do not require further analysis, and the system is simple and reliable.

**3.1. Spectrometer design**

In this section the principles followed during the design phase of the photon energy spectrometer, as well as the constraints limiting the options, are reported and discussed.

**3.1.1. VLS equations.** As mentioned in the previous sections the diffractive optical elements are three flat VLS gratings. Despite the flat substrate, the diffracted beam is focused because of the groove density variation. In fact, the groove density increases along the tangential direction of the grating. As a consequence, different diffraction angles occur on different parts of the grating and focusing in the tangential direction occurs. The VLS groove density can be expanded in the power series

$$N(w) = D_0 + D_1w + D_2w^2 + D_3w^3 + \dots \quad (1)$$

as a function of the tangential local coordinate  $w$  (centered at the grating pole) and is expressed in lines  $\text{mm}^{-1}$  (often referred as grooves  $\text{mm}^{-1}$ ).  $D_0$  is the central groove density equal to  $N(0)$ ,  $D_1$  is the linear variation,  $D_2$  is the quadratic variation, and so on. The optical path function  $F$  for a plane

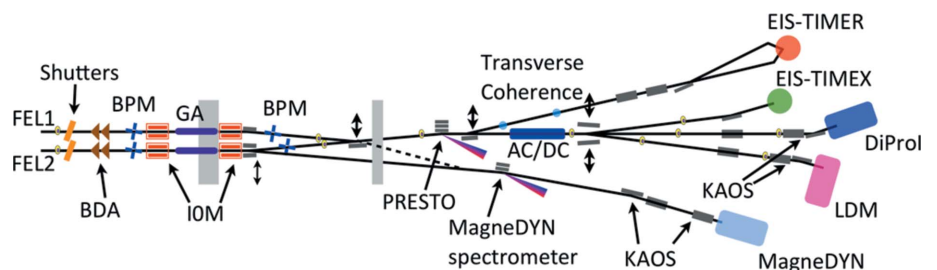


**Figure 1**  
Layout of the photon beam transport system of FERMI. From left to right, shutters, beam-defining apertures (BDA), beam position monitors (BPM), radiation intensity monitors (IO), gas absorbers (GA), three plane mirrors inside the safety hatch, Ce:YAG screens, photodiode-YAG-diagnostics (PYD), the on-line photon energy spectrometer (PRESTO), the auto correlator-delay creator (AC/DC) and, when inserted, the transverse coherence measurement system. Three of the five beamlines employ the Kirkpatrick–Baez active optic system (KAOS).

**Table 2**  
Spectrometer gratings parameters.

The low-energy grating is named as G1, the medium energy is G2 while the high-energy grating is G3.

Parameter	G1	G2	G3
Wavelength (energy) range, $m = 1$ [nm (eV)]	100–24.8 (12–50)	27.6–6.7 (45–185)	12.7–3.1 (98–400)
Wavelength (energy) range, $m = 2$ [nm (eV)]	24.8–12.4 (24–100)	13.9–3.4 (89–370)	6.3–1.55 (196–800)
Energy resolution (meV)	0.2–3.7	0.3–9.5	0.4–8.1
$D_0$ (grooves $\text{mm}^{-1}$ )	500	1800	3750
$D_1$ (grooves $\text{mm}^{-2}$ )	0.35	1.26	2.68
$D_2$ (grooves $\text{mm}^{-3}$ )	$1.7 \times 10^{-4}$	$6.3 \times 10^{-4}$	$1.4 \times 10^{-3}$
Groove profile	Laminar	Laminar	Laminar
Groove height (nm)	12	4	8
Groove ratio ( $w/d$ )	0.60	0.65	0.65
Coating material / thickness (nm)	Amorphous carbon / 50	Gold / 50	Nickel / 50

VLS grating can be expressed as a power series too, and the most important terms are (Peatman, 1997):  $F_{100}$ , the grating equation;  $F_{020}$ , the sagittal focus;  $F_{200}$ , the tangential focus; and  $F_{300}$ , the primary coma. The constant incidence angle  $\alpha$  has been chosen to be  $87.5^\circ$  (with respect to the normal direction of the grating) in order to have a high efficiency at the zeroth-order (reflected beam to the users) and to accept more than  $3\sigma$  of the incoming photon beam at wavelengths below 50 nm,

$$\begin{aligned}
 F_{100} &= mN\lambda - (\sin \alpha - \sin \beta), \\
 F_{200} &= \frac{1}{2} \left[ -mD_1\lambda + \left( \frac{\cos^2 \alpha}{r} + \frac{\cos^2 \beta}{r'} \right) \right], \\
 F_{020} &= \frac{1}{r} + \frac{1}{r'}, \\
 F_{300} &= -\frac{1}{3}mD_2\lambda + \frac{1}{2} \left( \frac{\cos^2 \alpha \sin \alpha}{r^2} + \frac{\cos^2 \beta \sin \beta}{r'^2} \right).
 \end{aligned} \tag{2}$$

The source distance  $r$  is assumed to be constant (57.5 m for FEL-1 and 49.9 m for FEL-2) considering the waist position inside the last undulator. Having fixed  $\alpha$  and  $r$ , the position of the focal point is a function of the photon wavelength only. The set of all the focal points is a curve in the dispersion plane

called the focal curve, which can be calculated defining the grating coefficients and knowing  $\alpha$  and  $r$  by using the previous formulas. In order to allow the placement of the detector at different focal points, the spectrometer has a movable exit arm capable of moving in both radial ( $r'$ ) and angular ( $\beta$ ) directions (Fig. 2, left). The minimum angle of diffraction allowed by the mechanical design of the instrument is about  $9.2^\circ$ , while the maximum is  $18.4^\circ$ , giving an angular span of about  $9.2^\circ$ . The minimum and maximum exit arm lengths are 2550 mm and 3050 mm, for a total excursion of 500 mm. Both these

movements are remotely controlled with micrometric precision. The spectral distribution is obtained by using the first, second or third diffraction order of the used grating.

**3.1.2. PRESTO parameters.** The system takes advantage of three VLS flat gratings. The main parameters and performances are summarized in Table 2. The substrates are 250 mm long, 25 mm wide and 40 mm thick (not cooled since the deposited power is low and a thermal bump does not occur). The grating patterns have been holographically ruled in the central  $60 \text{ mm} \times 20 \text{ mm}$ . The low-energy grating (G1) covers the wavelength range from 24.8 nm to 100 nm (12–50 eV) in the first diffraction order ( $m = 1$ ), while the second and third orders can be used to reach 8 nm (155 eV). The medium-energy grating (G2) is able to measure from 27.6 nm to 6.7 nm (45–185 eV) in the first order and, using the second and third orders, down to 2.2 nm (560 eV). The high-energy grating (G3) covers the range from 12.7 nm to 3.1 nm (98–400 eV) in the first order of diffraction and down to 1.03 nm (1200 eV) by using the second and third order.

The grating profiles have been chosen in order to guarantee low efficiency in the diffraction orders, *i.e.* to the detector. In this way almost all the radiation is efficiently transported to

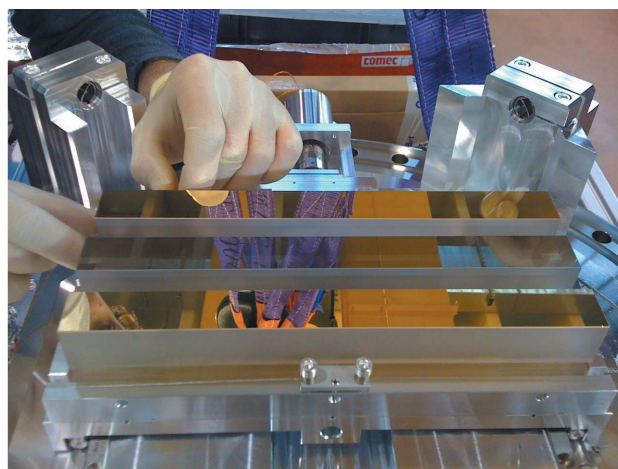
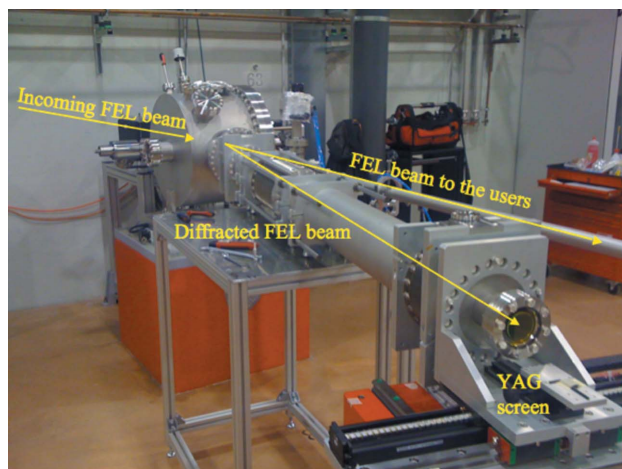


**Figure 2**

Left: photograph of the vacuum chamber hosting the diffraction gratings and the movable detector. Right: photograph of the low-energy, medium-energy and high-energy gratings mounted on the holder.

the experimental end-stations as explained in §3. The gratings are mounted parallel, one above the other, in a holder limiting the substrate distortions, preventing undesired aberrations. The in-vacuum motorized holder allows the vertical translation, to switch the gratings, and the rotation of pitch and roll, while the other movements have to be performed by acting directly on the vacuum chamber. A photograph of the holder hosting the gratings is shown in Fig. 2 (right).

The detection system is composed of a Ce:YAG crystal coupled with a cooled charge coupled device (CCD) camera. The Ce:YAG crystal is placed in a vacuum, glued on a viewport and converts the VUV/soft X-rays into visible light with an efficiency from 35% up to 80%, depending on the radiation wavelength. Right before the Ce:YAG, a retractable aluminium filter can be inserted in order to attenuate the beam intensity, followed by a manual valve that allows the Ce:YAG crystal to be replaced when needed without breaking the vacuum in the grating chamber. The CCD camera is produced by Hamamatsu Photonics (C8800 series) and is endowed with a  $1000 \times 1000$  pixels-chip with quantum efficiency from 30% up to 50% in the visible range.

The detector is placed in front of the viewport (in air) and the radiation emitted by the Ce:YAG crystal is focused onto the CCD chip by using a lens system. Two orthogonal translation stages permit the detector to be moved along the focal curves.

#### 4. Features and results

The PRESTO allows measurement on-line and shot-to-shot of the energy distribution of the FEL radiation permitting in real time the spectral distribution to be determined. Moreover, the spatial intensity distribution and the angular divergence can be monitored on-line as well, thanks to its peculiar features, as explained in detail the following paragraphs.

##### 4.1. Efficiency

The determination of the grating profiles (groove shape and parameters in terms of groove height and ratio) as well as the choice of the coatings has been performed by calculating the efficiency at various orders of diffraction. From the diffraction grating theory it is known that different groove profiles influence the efficiencies at various diffraction orders. Since the spectrometer is an on-line diagnostic (non-invasive), the intensity of the diffracted radiation has to be as low as possible (differently from a standard monochromator), but high enough to obtain a detectable signal at the detector. In order to check the consistency of the outputs, the efficiency has been calculated using two different codes: *REFLEC* (Schäfers, 1996) and *LUMNAB* (Nevière *et al.*, 1974). The results are in good agreement, with difference below 5%. The results obtained by using *REFLEC* are shown in Fig. 3. The profile better matching the requests, and available from the state-of-the-art manufacturing techniques, has been found to be the laminar one: it gives a relatively low efficiency as compared with that of a blaze shape, which on the contrary maximizes

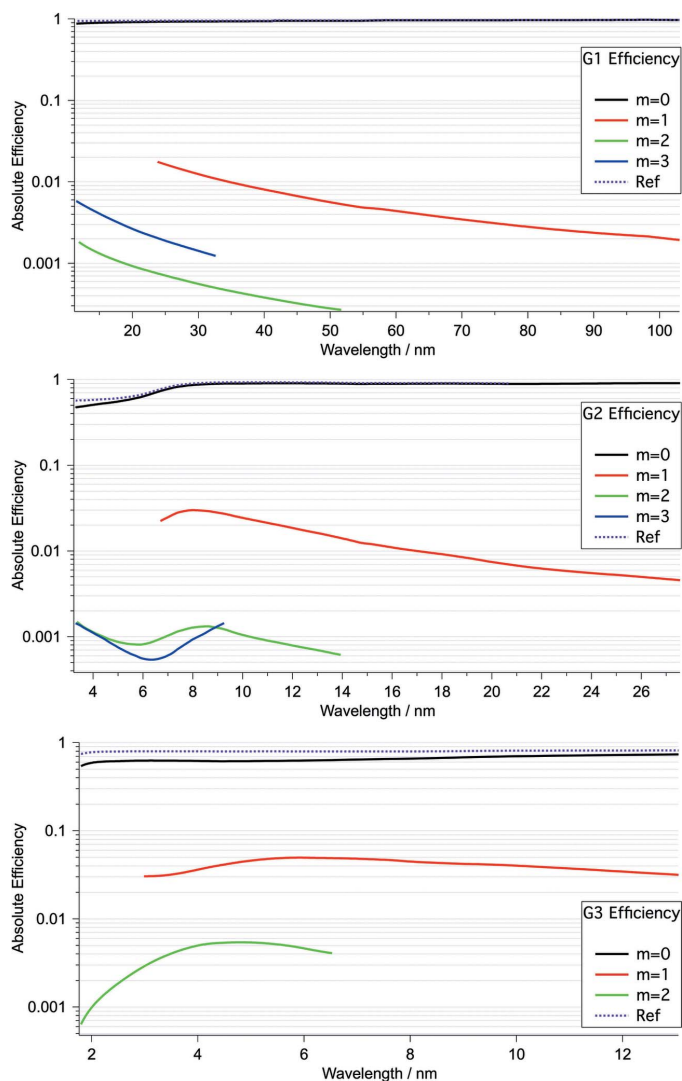


**Figure 3** Grating efficiency at the zeroth ( $m = 0$ , black), first ( $m = 1$ , red), second ( $m = 2$ , green) and third ( $m = 3$ , blue) orders of diffraction for the low- (G1, up), medium- (G2, centre) and high-energy (G3, bottom) gratings over the whole FERMI wavelength range. The intensity used for the measurement of the spectrum is much lower than the total radiation delivered to the users (zeroth order,  $m = 0$ , black), which is about 96–98% of the incoming photons. If the harmonic components have enough intensity then it is possible to use the second/third order of diffraction to perform single-shot spectral measurements. The purple dotted lines correspond to the reflectivity of a single mirror with the same coating and incidence angle as the gratings.

the efficiency at the first order of diffraction reducing the intensity of the zeroth order. In Table 2 the groove heights and ratios for the low- (G1), medium- (G2) and high-energy (G3) gratings are reported together with their working energies at different diffraction orders. The coatings have been chosen to be 50 nm single layers of amorphous-carbon (a-C) for G1, gold (Au) for G2 and nickel (Ni) for G3. The expected efficiencies are well below 5%, and the photon beam transmission to the end-stations is very close to the reflectivity in the case of plane mirrors, as shown in Fig. 3. For this reason PRESTO can work on-line without significantly disturbing the photon beam transported to the end-stations.

#### 4.2. Resolving power (theoretical versus experimental)

The grating groove density has been chosen in order to provide high resolution within the working spectral range. The resolving power has been evaluated considering the combined contribution of the gratings and the detector. The grating contribution has been evaluated adopting the Rayleigh criterion (the minimum resolvable energy at the focus of two different energies) by performing ray-tracing simulations with the *SHADOW* code (Cerrina *et al.*, 1994) taking into account the ideal and measured substrate shape and roughness, obtained after the metrological investigation, as explained in detail by Svetina *et al.* (2011).

The detector spatial resolution has been simulated by considering the finite pixel size of the CCD imaged over the Ce:YAG screen by the lens used [with a field of view (FoV) of 15.4 mm]. It has resulted in the latter being the main cause of the final resolution of the instrument which ranges between  $1.5 \times 10^4$  and  $3 \times 10^4$ .

The resolving power can be increased by using a different lens with a smaller FoV by losing intensity. The simulated resolving powers by considering the grating contribution only, and those obtained considering also the finite spatial resolution of the detector, are reported in Fig. 4. In the same figure are reported the measured resolving powers as obtained by data acquisitions performed during beam time at FERMI in RUN 9. By changing the FEL wavelength, by steps of 0.1 nm, it has been possible to measure the actual spectrometer resolution in a fraction of the FEL-1 wavelength range (26–52 nm, *i.e.* 24–48 eV) at the first order of diffraction. In fact, as explained by Allaria *et al.* (2012b), once the electron energy and the undulator gaps are fixed, the FEL process is driven by the seed laser wavelength that can be accordingly finely tuned using the third harmonic of the Ti:sapphire amplifier. This operation provides a variation in the seed laser wavelength of up to 0.4%. By measuring the transverse relative variation in the positioning of the spectral peak it has been possible to determine the spectrometer resolution, and to derive the actual resolving power (Fig. 5, top). The resolving power was found to be slightly lower than expected; nevertheless, its value is higher than  $10^4$ , high enough to resolve the FERMI spectral distribution with the requested accuracy. These measurements have confirmed that the theoretical resolving power is mainly reduced by the finite size of the CCD pixel. The measured bandwidths have been compared with measurements performed simultaneously tuning the seed laser, and scanning the wavelength across the  $1s-4p$  resonance in He atoms at 52.2 nm, detecting both the UV–visible fluorescence ( $4p-2s$  occurring at 400 nm) and EUV fluorescence ( $4p-1s$  occurring at 52.2 nm), as explained in more detail by Allaria *et al.* (2012b). The bandwidths have been found to be in agreement, confirming the proper calibration of the PADReS spectrometer (Fig. 5, bottom).

#### 4.3. Zeroth-order delivered to the end-stations

The zeroth-order, *i.e.* the reflected beam, is delivered to the experimental end-stations. For this reason, the photon beam

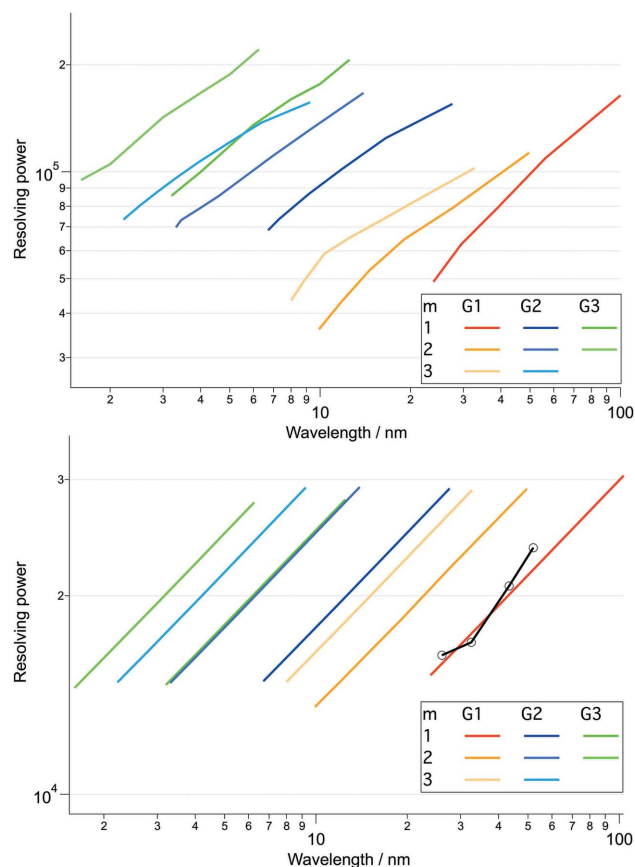


**Figure 4**

Simulated gratings (top) and total (bottom) resolving power for the three gratings of PRESTO at the different orders of diffraction. The drop in resolution is due to the used objective with a large FoV (15.4 mm) in order to collect the entire diffracted photon beam. The black line represents the measurements performed scanning the wavelength of the seed laser using an optical parametric amplifier.

shall not be perturbed in terms of intensity or wavefront. The relative variation between the efficiency at the zeroth-order of diffraction (coming from the ruled part of the optical surface of the gratings) and the reflectivity (coming from the non-ruled mirror-like sides of the same surfaces) is less than 1% as can be seen by comparing the black (efficiency) and purple (reflectivity) curves in Fig. 3. This slight difference is negligible for the end users, especially at lower wavelengths where the beam footprint on the surface is small and only the tails are reflected by the not-ruled area.

A wavefront deformation is expected in the presence of shape errors and micro-roughness, but it can also be a consequence of a periodic structure; *e.g.* the grating grooves. Since PRESTO gratings are flat, the wavefront is preserved, except for the presence of shape errors and micro-roughness in the substrate surface. Nonetheless, their effect is negligible since their value is well below  $0.4 \mu\text{rad}$  r.m.s. in the long-wavelength range, and micro-roughness  $\sigma$  less than  $1 \text{ \AA}$ . An estimation of the peak-to-valley distortion ( $P_tV$ ) of the wavefront caused by the grooves can be easily computed considering the variation of the optical path for a photon beam reflected by a laminar profile with groove height  $h$  and grazing incidence angle  $\alpha$ :

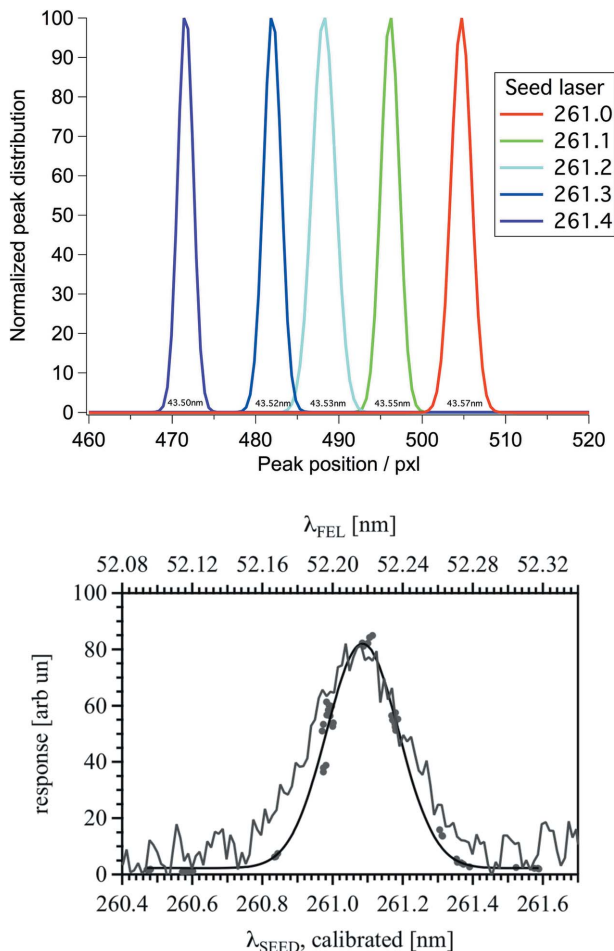


**Figure 5**  
 Top: example of the spectral peak shift due to the variation of the seed laser wavelength using an optical parametric amplifier. These data have been used for the experimental determination of the PRESTO resolving power with good agreement with respect to the simulations. Bottom [reproduced from Allaria *et al.* (2012), *New J. Phys.* **14**, 113009; Copyright 2012, Institute of Physics]: reconstructed He absorption profile scanning the wavelength across the  $1s-4p$  resonance at 52.2 nm ( $\lambda_{\text{FEL}} = \lambda_{\text{SEED}}/5$ ). Dots: photomultiplier response *versus* calibrated wavelength. The comparison between the Gaussian fit of the He signal with a single-shot acquired by PRESTO confirms both the FEL bandwidth and the spectrometer calibration.

$$P_t V = h \frac{1 - \cos(2\alpha)}{\sin \alpha} \quad (3)$$

The distortion of the wavefront is therefore mostly negligible since  $P_t V$  is 1.05 nm for G1, 0.35 nm for G2 and 0.70 for G3, which corresponds to a local deformation smaller than  $\lambda/50$  at 50 nm for G1,  $\lambda/30$  at 10 nm for G2, and  $\lambda/10$  at 7 nm for G3. From these results it is clear that the wavefront is sensitive to the presence of the high-energy grating due to the short wavelengths involved. We have investigated its effect with physical optics simulations performed using the *WISE* (Raimondi & Spiga, 2015) code. The obtained results have confirmed that the Strehl ratio after the reflection over the high-energy grating is well above 0.48 at wavelengths longer than 5 nm. This value drops to 0.65 at 3 nm even though an actual degradation of the wavefront has not been observed. In

any case, from the experience of the first experimental runs at FERMI it is clear that PRESTO is transparent for users over most of the FERMI wavelength range.

#### 4.4. Additional features: beam profile measurements and divergence estimation

The PRESTO VLS gratings have a non-zero  $F_{020}$  term (sagittal focus), thus the beam is focused in the tangential plane only. We can take advantage of this peculiarity by considering not only the horizontal distribution (*i.e.* the spectral content) but also the vertical one, which is the projection of the photon beam transverse profile. The measurement of the vertical distribution allows the use of PRESTO as a (partial) on-line screen. In fact, as the FERMI FEL radiation has been proven to present circular transverse emission symmetry, the vertical profile measured with the spectrometer is actually the projection of the FEL transverse intensity distribution. In Fig. 6 a graphical explanation of this feature is presented for different intensity distributions ( $\text{TEM}_{00}$ , hollow and a mix of modes) impinging over the spectrometer optics. The measured diffracted spots at the detector are compared with the footprints on the gratings. Once the vertical dimension/distribution is known, it is then possible to extract the beam divergence, just taking into account the distance between the detector and the last undulator. After having taken a set of images at two different screens and having calculated the angular divergence, a very good agreement with the theoretical values (Table 1) was found, meaning that PRESTO provides direct information

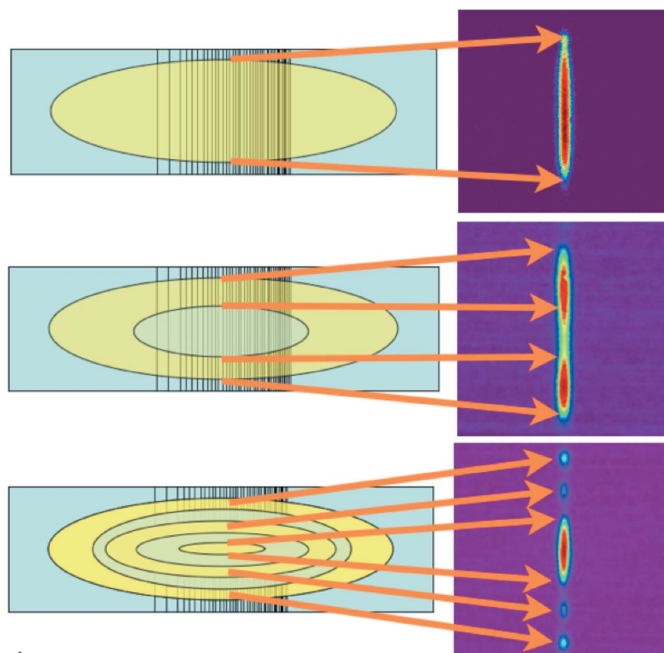


**Figure 6**  
 FEL intensity distribution as seen at the spectrometer detector. Top: a perfect Gaussian beam is emitted by the FEL and its vertical projection is seen as a Gaussian. Centre: a hollow mode caused by an off-resonant condition of the undulators is projected as two vertical peaks. Bottom: a set of mixed modes (Gaussian and hollows) is seen as a central Gaussian and some vertical satellites.

about the beam divergence without the need to insert any screen blocking the beam.

#### 4.5. Two-colour double-pulse measurements (spectrum and time delay)

One of the unique properties of FERMI is the possibility to generate multiple X-ray pulses, used for pump-probe experiments (De Ninno *et al.*, 2013; Mahieu *et al.*, 2013). This has been accomplished by seeding the electron bunch with two independent ultraviolet seed pulses, with a slightly shifted central wavelength, both tunable in the 260–262 nm range. In this way two independent FEL pulses have been generated at the seventh harmonic of the seed lasers (around 37.1 nm and 37.3 nm) with a variable temporal separation from 300 fs up to 700 fs (the limitations with this method are due to the electron bunch length, the upper limit being around 1 ps, and the seed pulse duration, the lower limit being 150 fs) (Allaria *et al.*, 2013b). Besides the regular determination of the spectral content of the two FEL pulses, PRESTO has been used for two additional tasks: to measure the relative intensity of the pulses, and to help in the determination of the temporal separation between pump and probe. The measurement of the former is non-trivial since the pulses are separated well below 1 ps, and, in general, an ultra-fast diagnostics system would be required. Unfortunately, the signals generated in the gas-based I0 monitor by the two pulses cannot be distinguished. However, comparing the area subtended by both spectra as measured by PRESTO we have been able to measure the relative intensity between the pulses, with high accuracy and on-line, on a shot-to-shot basis. The temporal separation has been controlled by scanning the delay between the two seed pulses and looking at the resulting FEL spectra of the double emission. In Fig. 7 a series of spectral distributions is shown as a function of the relative time delay between the seed lasers and the electron bunch. In the same figure besides the independent onset of the two FEL pulses, it can be seen that the central wavelength separation between the two pulses was about 0.2 nm with a relative time delay of 500 fs, a bandwidth RMS about 0.05% of the central wavelength, and a shot-to-shot peak position RMS jitter of about 0.005% of the central wavelength position.

## 5. Conclusions

PRESTO is currently operative and routinely used as the diagnostic dedicated to the measurement of the FERMI FEL photon beam spectral distribution and content. It is capable of measuring on-line and shot-to-shot, making the requested information immediately available to the users. The commissioning of the low- and medium-energy gratings has been carried out, while that of the high-energy grating is still ongoing. The performance expected from the simulations made in the design phase is very close to the actual one, especially in terms of resolving power. Additional features allow the photon beam transverse distribution and angular divergence to be measured, on-line and shot-to-shot. An indirect

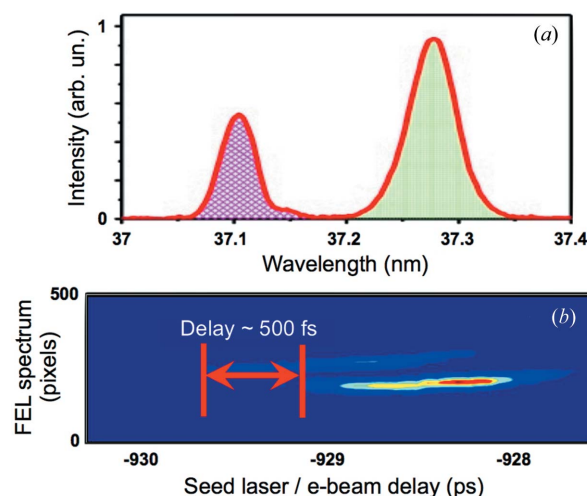


Figure 7

Top: spectral content and intensities of the pump (right) and probe (left) pulses measured with PRESTO in the two-color double-pulse experiment. Comparing the subtended areas it has been possible to measure on-line and shot-to-shot the relative intensities. Bottom: spectra of both pulses while scanning the relative time delay between the electron beam and the seed laser pulses. The pulse duration was around 50 fs while the separation between the pump-probe has been kept fixed at 500 fs.

measurement of the FEL intensity is also possible. Both the fundamental and the higher harmonics of the FEL emission have been measured with the low-, medium- and high-energy gratings. In this way it has been possible to determine the third-harmonic parameters in terms of beam size, divergence, intensity and bandwidth. It has been observed that the third-harmonic components have the expected characteristics both in bandwidth (around three times larger compared with the fundamental) and divergence (one third of the fundamental) while the intensity ranges from 0.1% to a few percent of the fundamental, depending on the machine settings. A preliminary campaign of characterization of the high-energy grating has been recently carried out and the results seem to indicate that the resolving power is as expected. Evidence of the third-harmonic component at 1.3 nm has been measured (the fundamental was set at 4 nm, FEL2), and will be the subject of a future paper.

## Acknowledgements

The authors would like to thank all colleagues having participated in the commissioning of PRESTO, and in particular the FERMI Commissioning Team and the experimental groups (DiProI, EIS-TIMEX and LDM). We would also like to thank all of the useful feedback given by external users who have permitted the improvement of the spectrometer performances.

## References

- Allaria, E., Appio, R., Badano, L., Barletta, W. A., Bassanese, S., Biedron, S. G., Borga, A., Busetto, E., Castronovo, D., Cinquegrana, P., Cleva, S., Cocco, D., Cornacchia, M., Craievich, P., Cudin, I., D'Auria, G., Dal Forno, M., Danailov, M. B., De Monte, R., De Ninno, G., Delgiusto, P., Demidovich, A., Di Mitri, S., Diviacco, B.,

- Fabris, A., Fabris, R., Fawley, W., Ferianis, M., Ferrari, E., Ferry, S., Froehlich, L., Furlan, P., Gaio, G., Gelmetti, F., Giannessi, L., Giannini, M., Gobessi, R., Ivanov, R., Karantzoulis, E., Lonza, M., Lutman, A., Mahieu, B., Milloch, M., Milton, S. V., Musardo, M., Nikolov, I., Noe, S., Parmigiani, F., Penco, G., Petronio, M., Pivetta, L., Predonzani, M., Rossi, F., Rumiz, L., Salom, A., Scafuri, C., Serpico, C., Sigalotti, P., Spampinati, S., Spezzani, C., Svandrlík, M., Svetina, C., Tazzari, S., Trovo, M., Umer, R., Vascotto, A., Veronese, M., Visintini, R., Zaccaria, M., Zangrando, D. & Zangrando, M. (2012a). *Nat. Photon.* **6**, 699–704.
- Allaria, E., Badano, L., Bassanese, S., Capotondi, F., Castronovo, D., Cinquegrana, P., Danailov, M. B., D’Auria, G., Demidovich, A., De Monte, R., De Ninno, G., Di Mitri, S., Diviacco, B., Fawley, W. M., Ferianis, M., Ferrari, E., Gaio, G., Gauthier, D., Giannessi, L., Iazzourene, F., Kurdi, G., Mahne, N., Nikolov, I., Parmigiani, F., Penco, G., Raimondi, L., Rebernik, P., Rossi, F., Roussel, E., Scafuri, C., Serpico, C., Sigalotti, P., Spezzani, C., Svandrlík, M., Svetina, C., Trovò, M., Veronese, M., Zangrando, D. & Zangrando, M. (2015). *J. Synchrotron Rad.* **22**, 485–491.
- Allaria, E., Battistoni, A., Bencivenga, F., Borghes, R., Callegari, C., Capotondi, F., Castronovo, D., Cinquegrana, P., Cocco, D., Coreno, M., Craievich, P., Cucini, R., D’Amico, F., Danailov, M. B., Demidovich, A., De Ninno, G., Di Cicco, A., Di Fonzo, S., Di Fraia, M., Di Mitri, S., Diviacco, B., Fawley, W. M., Ferrari, E., Filipponi, A., Froehlich, L., Gessini, A., Giangrisostomi, E., Giannessi, L., Giuressi, D., Grazioli, C., Gunnella, R., Ivanov, R., Mahieu, B., Mahne, N., Masciovecchio, C., Nikolov, I. P., Passos, G., Pedersoli, E., Penco, G., Principi, E., Raimondi, L., Sergo, R., Sigalotti, P., Spezzani, C., Svetina, C., Trovò, M. & Zangrando, M. (2012b). *New J. Phys.* **14**, 113009.
- Allaria, E., Bencivenga, F., Borghes, R., Capotondi, F., Castronovo, D., Charalambous, P., Cinquegrana, P., Danailov, M. B., De Ninno, G., Demidovich, A., Di Mitri, S., Diviacco, B., Fausti, D., Fawley, W. M., Ferrari, E., Froehlich, L., Gauthier, D., Gessini, A., Giannessi, L., Ivanov, R., Kiskinova, M., Kurdi, G., Mahieu, B., Mahne, N., Nikolov, I., Masciovecchio, C., Pedersoli, E., Penco, G., Raimondi, L., Serpico, C., Sigalotti, P., Spampinati, S., Spezzani, C., Svetina, C., Trovò, M. & Zangrando, M. (2013b). *Nat. Commun.* **4**, 2476.
- Allaria, E., Callegari, C., Cocco, D., Fawley, W. M., Kiskinova, M., Masciovecchio, C. & Parmigiani, F. (2010). *New J. Phys.* **12**, 075002.
- Allaria, E., Castronovo, D., Cinquegrana, P., Craievich, P., Dal Forno, M., Danailov, M. B., D’Auria, G., Demidovich, A., De Ninno, G., Di Mitri, S., Diviacco, B., Fawley, W. M., Ferianis, M., Ferrari, E., Froehlich, L., Gaio, G., Gauthier, D., Giannessi, L., Ivanov, R., Mahieu, B., Mahne, N., Nikolov, I., Parmigiani, F., Penco, G., Raimondi, L., Scafuri, C., Serpico, C., Sigalotti, P., Spampinati, S., Spezzani, C., Svandrlík, M., Svetina, C., Trovo, M., Veronese, M., Zangrando, D. & Zangrando, M. (2013a). *Nat. Photon.* **7**, 913–918.
- Allaria, E., Diviacco, B., Callegari, C., Finetti, P., Mahieu, B., Viehhaus, J., Zangrando, M., De Ninno, G., Lambert, G., Ferrari, E., Buck, J., Ilchen, M., Vodungbo, B., Mahne, N., Svetina, C., Spezzani, C., Di Mitri, S., Penco, G., Trovò, M., Fawley, W. M., Rebernik, P. R., Gauthier, D., Grazioli, C., Coreno, M., Ressel, B., Kivimäki, A., Mazza, T., Glaser, L., Scholz, F., Seltmann, J., Gessler, P., Grünert, J., De Fanis, A., Meyer, M., Knie, A., Moeller, S. P., Raimondi, L., Capotondi, F., Pedersoli, E., Plekan, O., Danailov, M. B., Demidovich, A., Nikolov, I., Abrami, A., Gautier, J., Lüning, J., Zeitoun, P. & Giannessi, L. (2014). *Phys. Rev. X*, **4**, 041040.
- Brenner, G., Kapitzi, S., Kuhlmann, M., Ploenjes, E., Noll, T., Siewer, F., Treusch, R., Tiedtke, K., Reiningner, R., Roper, M. D., Bowler, M. A., Quinn, F. M. & Feldhaus, J. (2011). *Nucl. Instrum. Methods Phys. Res. A*, **635**, S99–S103.
- Cerrina, F., Welna, C., Chen, G. J. & Sanchez del Rio, M. (1994). *SHADOW PRIMER*. Center for X-ray Lithography, University of Wisconsin, Wisconsin, USA.
- De Ninno, G., Mahieu, B., Allaria, E., Giannessi, L. & Spampinati, S. (2013). *Phys. Rev. Lett.* **110**, 064801.
- Finetti, P., Allaria, E., Diviacco, B., Callegari, C., Mahieu, B., Viehhaus, J., Zangrando, M., De Ninno, G., Lambert, G., Ferrari, E., Buck, J., Ilchen, M., Vodungbo, B., Mahne, N., Svetina, C., Spezzani, C., Di Mitri, S., Penco, G., Trovò, M., Fawley, W. M., Rebernik, P., Gauthier, D., Grazioli, C., Coreno, M., Ressel, B., Kivimäki, A., Mazza, T., Glaser, L., Scholz, F., Seltmann, J., Gessler, P., Grünert, J., De Fanis, A., Meyer, M., Knie, A., Moeller, S. P., Raimondi, L., Capotondi, F., Pedersoli, E., Plekan, O., Danailov, M., Demidovich, A., Nikolov, I., Abrami, A., Gautier, J., Lüning, J., Zeitoun, P. & Giannessi, L. (2014). *Proc. SPIE*, **9210**, 92100K.
- Mahieu, B., Allaria, E., Castronovo, D., Danailov, M. B., Demidovich, A., De Ninno, G., Di Mitri, S., Fawley, W. M., Ferrari, E., Fröhlich, L., Gauthier, D., Giannessi, L., Mahne, N., Penco, G., Raimondi, L., Spampinati, S., Spezzani, C., Svetina, C., Trovò, M. & Zangrando, M. (2013). *Opt. Express*, **21**, 22728–22741.
- Nevière, M., Vincent, P. & Petit, R. (1974). *Nouv. Rev. Opt.* **5**, 65.
- Peatman, W. B. (1997). *Gratings, Mirrors and Slits: Beamline Design for Soft X-ray Synchrotron Radiation Sources*. New York: Gordon & Breach.
- Raimondi, L. & Spiga, D. (2015). *Astron. Astrophys.* **573**, A17.
- Rumiz, L., Cocco, D., Fava, C., Gerusina, S., Gobessi, R., Mazzucco, E., Zudini, F. & Zangrando, M. (2011). *Proceedings of the 2nd International Particle Accelerator Conference*, pp. 1530–1532.
- Schäfers, F. (1996). BESSY Technical Report 202/96. BESSY, Berlin, Germany.
- Svetina, C., Abrami, A., Cudin, I., Fava, C., Gerusina, S., Gobessi, R., Rumiz, L., Sostero, G., Zangrando, M. & Cocco, D. (2011). *Proc. SPIE*, **8139**, 81390J.
- Zangrando, M., Abrami, A., Bacescu, D., Cudin, I., Fava, C., Frassetto, F., Galimberti, A., Godnig, R., Giuressi, D., Poletto, L., Rumiz, L., Sergo, R., Svetina, C. & Cocco, D. (2009). *Rev. Sci. Instrum.* **80**, 113110.
- Zangrando, M., Cocco, D., Fava, C., Gerusina, S., Gobessi, R., Mahne, N., Mazzucco, E., Raimondi, L., Rumiz, L. & Svetina, C. (2015). *J. Synchrotron Rad.* **22**, 565–570.
- Zangrando, M., Fava, C., Gerusina, S., Gobessi, R., Mahne, N., Mazzucco, E., Raimondi, L., Rumiz, L. & Svetina, C. (2014). *Proc. SPIE*, **9210**, 921003.